Thermochimica Acta, 162 (1990) 265–275
Elsevier Science Publishers B.V., Amsterdam – Printed in The Netherlands

INFLUENCE OF OXYGEN PRESSURE ON OXIDATION–REDUCTION PHENOMENA OBSERVED WITH SUBMICROMETRE-SIZED MANGANESE-SUBSTITUTED MAGNETITES

B. GILLOT and M. EL GUENDOUZI

Faculté des Sciences Mirande, Laboratoire sur la Réactivité des Solides, associé au C.N.R.S., U.A. 23, B.P. 138, 21004 Dijon Cedex (France)

(Received 24 October 1989)

ABSTRACT

Over the temperature range 250–600 ° C, the oxidation of submicrometre-sized manganese-substituted magnetites depends on oxygen pressure because the presence of manganese ions leads to redox phenomena. Below 400 ° C, within the single-phase region of the cation-deficient spinel, a quantitative analysis by DTG of oxidizable cations allows the defect concentration associated with partial oxidation of manganese ions in tetrahedral sites to be related to oxygen pressure. Above 550 ° C, the oxidation of manganese ions not oxidized previously is accompanied by a structural change, but the nature of the inversion products again depends markedly on oxygen pressure.

INTRODUCTION

In a previous paper [1], the authors showed that the reactivity in air of submicrometre-sized manganese-substituted magnetites, $Fe_{3-x}Mn_xO_4$ ($0 < x < 1$), leads to complex phenomena associated with the charge and position of manganese ions in the spinel structure. Below 450 ° C, where the spinel structure was preserved, the differential thermogravimetric (DTG) curves, $d\Delta m/dt = f(t)$, show a three-stage oxidation process (region I) related to the distribution of Fe^{2+} and Mn^{3+} ions on octahedral sites and Mn^{2+} ions on tetrahedral sites. A quantitative analysis of cations from the determination of oxidation peak areas, based on this discrepancy in reactivity, indicates that octahedrally sited Fe^{2+} and Mn^{3+} ions are totally oxidized (at ca. 190 ° C and 270 ° C, respectively) whereas tetrahedrally sited Mn^{2+} ions exhibit only partial oxidation (at ca. 350 ° C). At higher temperatures (> 450 ° C), quantitative analysis has established that the Mn^{4+} ions formed at ca. 270 ° C are reduced to Mn^{3+} ions (region II). It was also found that the proportion of Mn^{2+} ions not oxidized at low temperatures reacted with air at ca. 550 ° C to produce Mn^{3+} ions (region III). This reaction is accompanied by a phase change from a cation-deficient spinel structure to a corundum structure.

In the present paper we focus on the influence of oxygen pressure on the oxidation and reduction behaviour of manganese-substituted magnetites with crystallite sizes less than 100 nm. The observed complex oxidation–reduction phenomena were correlated with the degree of oxidation of iron and manganese in the spinel structure and with the nature of phases formed during the decomposition of the spinel phase at high temperature.

SAMPLES AND EXPERIMENTAL METHOD

Samples

Submicrometre-sized manganese-substituted magnetites, $Fe_{3-x}Mn_xO_4$ with $0 < x < 1$, were prepared from oxalate precursor mixtures as described previously [2]. For these initial spinels, many investigations employing radiocrystallographic analysis and the saturation magnetic moment [3] have shown that the Mn^{2+} and Fe^{3+} ions are associated with tetrahedral sites (A sites) and that the Mn^{3+}, Fe^{2+} and Fe^{3+} ions are found on octahedral sites (B sites). Only the Fe^{3+} ions are distributed among sites of both types. From these investigations, the ion distribution in the spinel lattice at room temperature can be formulated as

$$(Mn^{2+}_{0.8x}Fe^{3+}_{1-0.8x})_A(Fe^{3+}_{1+0.6x}Fe^{2+}_{1-0.8x}Mn^{3+}_{0.2x})_BO_4^{2-}$$

A quantitative analysis in regions I, II and III of samples oxidized in air [4], achieved from the measurement of oxidation peak areas obtained by DTG, confirms this distribution. In this analysis the variation of the S_i/S_0 ratio, where S_i represents the area of each peak and S_0 the area of the peak corresponding to pure magnetite ($x = 0$), is indicative of the quantities of Fe^{2+}, Mn^{3+} and Mn^{2+} ions within the initial spinel.

Measurements

The samples were oxidized in a Setaram MT-B 10-8 microbalance operated at a constant rate of 2.5 °C min^{-1} from 20–700 °C at different oxygen pressures. The material weighed 6 mg and the powder was spread out so that it would be oxidized in the same way as N independent particles of equal mean radius. Before every reaction, great care had to be taken while degassing to ensure that the powder was not even partially oxidized. This necessitated a vacuum of $< 10^{-4}$ Pa and a very slow temperature rise, so that no mass change occurred during the heating period. Phases were analysed by X-ray diffraction of samples cooled from various temperatures in the TG apparatus.

RESULTS AND DISCUSSION

Influence of oxygen pressure on oxidation characteristics

The effect of oxygen pressure on oxidation–reduction phenomena is shown in Figs. 1 and 2 for the compositions $x = 0.37$ and $x = 0.97$. As already reported for oxidation in air ($P_{O_2} = 2 \times 10^5$ Pa), in region I the original spinel is oxidized to a cation-deficient spinel and the mass gain is due to total oxidation of Fe^{2+} ions (to Fe^{3+} ions) and Mn^{3+} ions (to Mn^{4+}

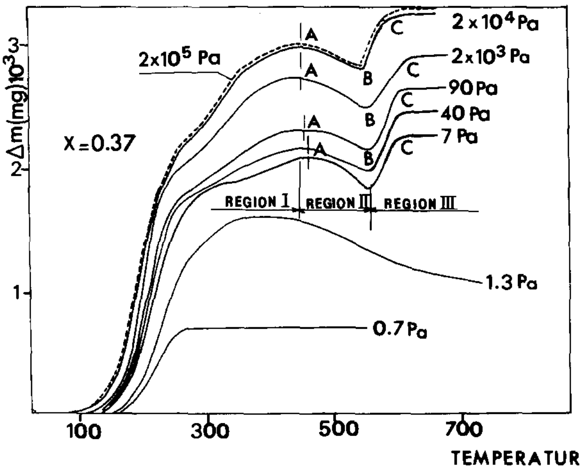

Fig. 1. Thermogravimetric curves for manganese-substituted magnetites heated at 2.5 °C min^{-1} at different oxygen pressures for $x = 0.37$.

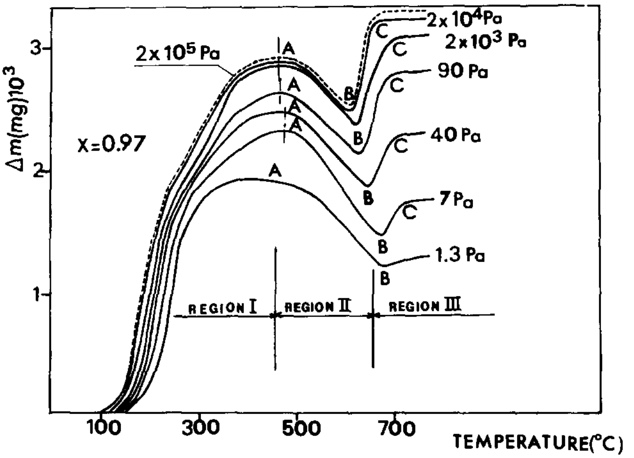

Fig. 2. Thermogravimetric curves for manganese-substituted magnetites heated at 2.5 °C min^{-1} at different oxygen pressures for $x = 0.97$.

ions) on B sites and incomplete oxidation of Mn^{2+} ions (to Mn^{3+} ions) on A sites. Above 400 °C, the compound starts to lose mass (region II), which corresponds to the reduction of Mn^{4+} to Mn^{3+} ions. For the two regions, X-ray diffraction shows a single phase of spinel structure. Above 550 °C (region III) there is again a mass gain due to the oxidation of Mn^{2+} ions that were incompletely oxidized at lower temperatures.

When the oxygen pressure is decreased, especially when the oxygen pressure in the environment during the oxidation is much lower than that in air, the maximum at point A is diminished as a result of the decrease in the amount of oxidized ions in region I. From point A, a further loss in mass occurs at higher temperature according to the reduction of manganese ions as shown in Figs. 1 and 2. However, the amount of reduced Mn^{4+} ions for the composition $x = 0.97$ seems more affected by the oxygen pressure, as the portion AB greatly increases with decreasing oxygen pressure (Fig. 2). Moreover, point B moves towards higher temperatures when the oxygen pressure is diminished. Above ca. 550 °C (region III), there is again a mass gain according to the oxidation of Mn^{2+} ions, but the magnitude of portion BC is found to decrease sharply, for $x = 0.97$, as the oxygen pressure decreases.

In order to make a systematic study of the oxidation process relative to oxygen pressure, quantitative analysis of cations from the determination of oxidation peak areas has been undertaken in each region.

Oxidation–reduction in region I

Quantitative analysis from DTG curves

An example of the effect of the distribution of Fe^{2+}, Mn^{3+} and Mn^{2+} ions between B and A sites and the effect of oxygen pressure were demonstrated directly for the composition $x = 0.37$ from DTG curves (Fig. 3). The oxidation proceeded through three distinct steps with a shift of the peak towards higher temperatures with decrease of oxygen pressure. From computer fitting, it appeared that the S_i/S_0 ratios of the first and second peaks (Table 1, columns 3 and 6) agree very well with the concentrations of Fe^{2+} and Mn^{3+} ions calculated from the structural formula (values in parentheses) for oxygen pressures above 100 Pa. It is only for oxygen pressures below 100 Pa that the area ratio has diminished to an appreciable degree, suggesting incomplete oxidation for these cations. On the other hand, whatever the oxygen pressure, the S_i/S_0 value corresponding to the third peak does not agree with the concentration of Mn^{2+} ions and is always lower than that calculated (Table 1, column 9), indicating a partial oxidation of Mn^{2+} ions.

From these results it appears that, for oxygen pressures above ca. 100 Pa, the variation of percentage oxidation at point A (Table 1, column 10) could be correlated with the amount of Mn^{2+} ions on A sites, which depends on

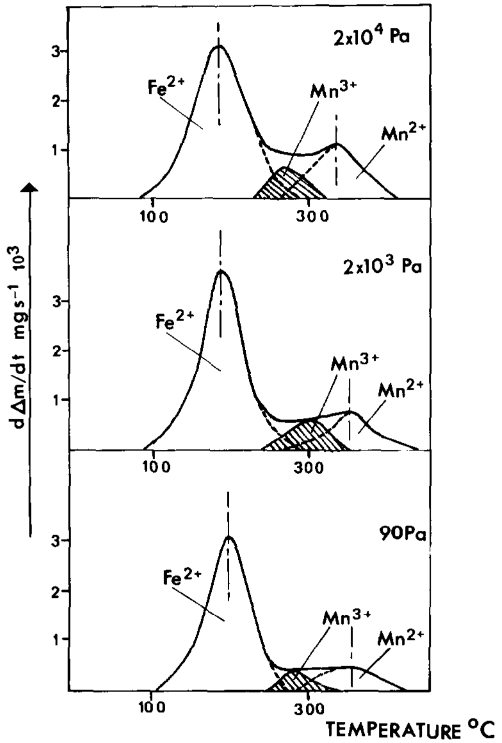

Fig. 3. Differential TG curves $dm/dt = f(T)$ in region I (———) and deconvolution spectra (– – –) of oxidation processes (Fe^{2+} and Mn^{3+} on B sites and Mn^{2+} ions on A sites) for sample with $x = 0.37$.

the extent of substitution and the oxygen pressure as shown in Fig. 4 (curves a and b).

Expression of the defect concentration

The cation-deficient manganese-substituted magnetites formed during the oxidation of the initial phases may be represented by the following reaction chain in the ionic notation of Kröger [5] by considering, as for Zn–Mn ferrites [6], that the predominant structural defects associated with deviations from stoichiometry are cation vacancies, V [2]:

$$\begin{aligned}&\tfrac{1}{2}(1-0.8x)\mathrm{O}_2 + 2(1-0.8x)\mathrm{Fe}_{\mathrm{Fe}_{\mathrm{II(B)}}}\\&\quad\rightarrow \tfrac{1}{4}(1-0.8x)\mathrm{V}''_{\mathrm{Fe}_{\mathrm{II(B)}}} + \tfrac{1}{4}(1-0.8x)\mathrm{Fe}^{\cdot}_{\mathrm{Fe}_{\mathrm{II(B)}}} + \tfrac{1}{2}(1-0.8x)\mathrm{V}'''_{\mathrm{Fe}_{\mathrm{III(B)}}}\\&\qquad + (1-0.8x)\mathrm{O}_0 \end{aligned}\tag{1}$$

$$\begin{aligned}&\tfrac{1}{2}(0.2x)\mathrm{O}_2 + 2(0.2x)\mathrm{Mn}_{\mathrm{Mn}_{\mathrm{III(B)}}}\\&\quad\rightarrow \tfrac{1}{4}(0.2x)\mathrm{V}''_{\mathrm{Mn}_{\mathrm{II(A)}}} + \tfrac{1}{2}(0.2x)\mathrm{V}'''_{\mathrm{Mn}_{\mathrm{III(B)}}} + 2(0.2x)\mathrm{Mn}^{\cdot}_{\mathrm{Mn}_{\mathrm{III(B)}}} + 0.2x\mathrm{O}_0\end{aligned}\tag{2}$$

$$\begin{aligned}&\tfrac{1}{2}(0.8bx)\mathrm{O}_2 + 2(0.8bx)\mathrm{Mn}_{\mathrm{Mn}_{\mathrm{II(A)}}}\\&\quad\rightarrow \tfrac{1}{4}(0.8bx)\mathrm{V}''_{\mathrm{Mn}_{\mathrm{II(A)}}} + 0.8bx\mathrm{V}'''_{\mathrm{Mn}_{\mathrm{III(B)}}} + 2(0.8bx)\mathrm{Mn}^{\cdot}_{\mathrm{Mn}_{\mathrm{II(A)}}} + 0.8bx\mathrm{O}_0\end{aligned}\tag{3}$$

TABLE 1

Dependence of S_i/S_0 ratio, oxidation percentage and oxidation temperature of each peak on the oxygen pressure in region I. The values in parentheses are those calculated from structural formulae

Oxygen pressure (Pa)	x	Region I								
		First peak			Second peak			Third peak		
		S_i/S_0	Fe^{2+} oxidized (%)	T_{ox} (°C)	S_i/S_0	Mn^{3+} oxidized (%)	T_{ox} (°C)	S_i/S_0	Mn^{2+} oxidized (%)	T_{ox} (°C)
2×10^5	0.37	0.69 (0.70)	99	184	0.07 (0.07)	100	270	0.20 (0.30)	66	340
	0.97	0.22 (0.23)	96	178	0.19 (0.19)	100	225	0.37 (0.77)	48	302
2×10^4	0.37	0.68	97	184	0.07	100	269	0.18	60	345
	0.97	0.22	96	180	0.19	100	225	0.35	45	305
2×10^3	0.37	0.68	97	186	0.07	100	290	0.13	43	348
	0.97	0.22	96	180	0.18	95	277	0.32	41	319
90	0.37	0.58	83	196	0.055	79	280	0.09	30	360
	0.97	0.21	91	185	0.17	89	305	0.28	38	350
40	0.37	0.55	78	200	0.06	85	320	0.07	23	384
	0.97	0.18	83	197	0.15	79	307	0.25	32	361

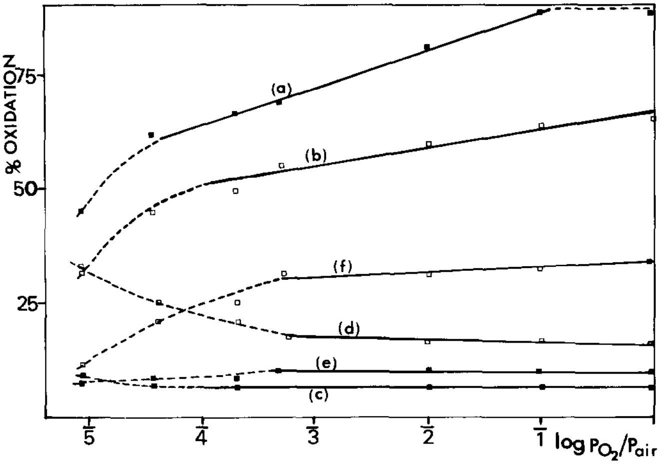

Fig. 4. Variation of the oxidation and reduction percentage in regions I, II and III determined from S_i/S_0 ratios as a function of oxygen pressure. ■, $x = 0.37$; □, $x = 0.97$. a and b, region I; c and d, region II; e and f, region III.

As was recalled previously, oxidation of Mn^{2+} ions in region I is only partial, and therefore a coefficient b is introduced into eqn. (3). The developed formula of the cation-deficient spinels can be written as

$$\begin{aligned}\tfrac{1}{2}(1-0.6x+0.8bx)\mathrm{O}_2 &+ 2(1-0.8x)\mathrm{Fe}_{\mathrm{Fe}_{\mathrm{II(B)}}} + 0.4x\mathrm{Mn}_{\mathrm{Mn}_{\mathrm{III(B)}}}\\ + 1.6bx\mathrm{Mn}_{\mathrm{Mn}_{\mathrm{II(A)}}} &\rightarrow \tfrac{1}{4}(1-0.8x)\mathrm{V}''_{\mathrm{Fe}_{\mathrm{II(B)}}} + \tfrac{1}{4}(0.2x)\mathrm{V}''_{\mathrm{Mn}_{\mathrm{II(A)}}}\\ &+ \tfrac{1}{4}(0.8bx)\mathrm{V}''_{\mathrm{Mn}_{\mathrm{II(A)}}} + \tfrac{1}{2}(1-0.8x)V'''_{\mathrm{Fe}_{\mathrm{III(B)}}}\\ &+ \tfrac{1}{2}(0.2x)\mathrm{V}'''_{\mathrm{Mn}_{\mathrm{III(B)}}} + \tfrac{1}{2}(0.8bx)\mathrm{V}'''_{\mathrm{Mn}_{\mathrm{III(B)}}}\\ &+ 2(1-0.8x)\mathrm{Fe}^{\bullet}_{\mathrm{Fe}_{\mathrm{II(B)}}} + 2(0.2x)\mathrm{Mn}^{\bullet}_{\mathrm{Mn}_{\mathrm{III(B)}}}\\ &+ 2(0.8bx)\mathrm{Mn}^{\bullet}_{\mathrm{Mn}_{\mathrm{II(A)}}} + \tfrac{1}{2}(1-0.6x+0.8bx)\mathrm{O}_0 \qquad (4)\end{aligned}$$

Under the assumptions that all point defects behave as ideal solutes in the crystal, the mass action law for eqn. (4) may be written as

$$\begin{aligned}K_1(P_{\mathrm{O}_2})^{\theta/2} = &\left|\mathrm{V}''_{\mathrm{Fe}_{\mathrm{II(B)}}}\right|^{\frac{1}{4}(1-0.8x)}\left|\mathrm{V}''_{\mathrm{Mn}_{\mathrm{II(A)}}}\right|^{\frac{1}{4}(0.2x+0.8bx)}\left|\mathrm{V}'''_{\mathrm{Mn}_{\mathrm{III(B)}}}\right|^{\frac{1}{2}(0.2x)}\\ &\times\left|\mathrm{V}'''_{\mathrm{Fe}_{\mathrm{III(B)}}}\right|^{\frac{1}{2}(1-0.8x+0.8bx)}\left|\mathrm{Fe}^{\bullet}_{\mathrm{Fe}_{\mathrm{II(B)}}}\right|^{2(1-0.8x)}\left|\mathrm{Mn}^{\bullet}_{\mathrm{Mn}_{\mathrm{II(B)}}}\right|^{0.4x}\\ &\times\left|\mathrm{Mn}^{\bullet}_{\mathrm{Mn}_{\mathrm{II(A)}}}\right|^{2(0.8bx)} \qquad (5)\end{aligned}$$

with $\theta = 1 - 0.6x + 0.8bx$. In addition, the relations expressing electroneutrality and concentration of vacancies, such as

$$2\left|\mathrm{M}^{\bullet}_{\mathrm{M}_{\mathrm{II(B)}}}\right| = \tfrac{1}{4}\left|\mathrm{V}''_{\mathrm{M}_{\mathrm{II(B)}}}\right| + \tfrac{1}{2}\left|\mathrm{V}'''_{\mathrm{M}_{\mathrm{III(B)}}}\right| \qquad (6)$$

$$\left.\begin{aligned}\left|\mathrm{V}'''_{\mathrm{M}_{\mathrm{III(B)}}}\right| &= 2\left|\mathrm{V}''_{\mathrm{M}_{\mathrm{II(A)}}}\right|\\ \left|\mathrm{V}''_{\mathrm{M}_{\mathrm{II(A)}}}\right| &= \left|\mathrm{V}''_{\mathrm{M}_{\mathrm{II(B)}}}\right|\end{aligned}\right\} \qquad (7)$$

allow the defect concentration to be related to the oxygen pressure. For eqn. (5), calculation gives

$$K_2\left(P_{O_2}\right)^{\theta/2} = |V_M|^{\frac{3}{4}\theta}|Fe^{\bullet}_{Fe_{II(B)}}|^{2(1-0.8x)}|Mn^{\bullet}_{Mn_{III(B)}}|^{0.4x}|Mn^{\bullet}_{Mn_{II(A)}}|^{2(0.8bx)} \quad (8)$$

Assuming that the oxidation of Fe^{2+} and Mn^{3+} ions is total at point A for oxygen pressures above ca. 100 Pa, the defect concentration corresponding to these two cations is a constant, and eqn. (8) can be written as

$$K_3\left(P_{O_2}\right)^{\theta/2} = \left|V_M^{\frac{3}{4}\theta}\right|\left|Mn^{\bullet}_{Mn_{II(A)}}\right|^{1.6bx} \quad (9)$$

For each composition x, the coefficient b corresponding to oxidized Mn^{2+} ions can be determined from the experimental values (Table 1, column 10), which shows also that the percentage of oxidized Mn^{2+} ions varies with the oxygen pressure.

Oxidation–reduction in regions II and III

Quantitative analysis

For these two regions, the S_i/S_0 ratio and the top temperature of the fourth (region II) and fifth peak (region III) versus oxygen pressure are listed in Table 2. It is only for oxygen pressures below 90 Pa that the S_i/S_0 values of the fourth peak, attributed to the reduction of Mn^{4+} to Mn^{3+} ions (Table 2, column 3), is not in agreement with the S_i/S_0 values of the second peak (Table 1, column 6), which is associated with oxidation of Mn^{3+} ions on octahedral sites. The reason for this is that the area of the fourth peak of reduction is probably caused also by a partial reduction of Mn^{3+} to Mn^{4+} ions. Figure 4 (curves c and d) shows the variation of the percentage of reduction corresponding to the portion AB. As the figure indicates, the effect of oxygen pressure on the reduction is more pronounced for low oxygen pressures, particularly for high extents of manganese substitution.

The reoxidized amount in region III is explained for oxygen pressures above 100 Pa by examining the S_i/S_0 ratio of the fifth peak (Table 2, column 6) and that of the third peak (Table 1, column 9). The total amount of oxidized Mn^{2+} ions can be determined from the sum of the S_i/S_0 ratios of column 6 (Table 2) and column 9 (Table 1). From these calculated values it can be seen that the total amount of oxidized Mn^{2+} ions is comparable with the concentration of Mn^{2+} ions calculated from the structural formula, which implies that the tetrahedral Mn^{2+} ions not completely oxidized in region I could be totally oxidized in region III. However, at low oxygen pressure, the percentage of oxidized ions in region III is diminished (Fig. 4, curves e and f) as a result of the decrease in the amount of oxidized Mn^{2+} ions.

Phase transformation of cation-deficient spinels

In region III, the oxidation of Mn^{2+} ions is accompanied by a phase transformation of the cation-deficient spinels, but the nature of the oxides

TABLE 2

Dependence of S_i/S_0 ratio, oxidation (or reduction) percentage, oxidation (or reduction) temperature on the oxygen pressure in regions II and III. The values in parentheses are those calculated from structural formulae

Oxygen pressure (Pa)	x	Region II Fourth peak			Region III Fifth peak		
		S_i/S_0	Mn^{4+} reduced (%)	T_{ox} (°C)	S_i/S_0	Mn^{2+} oxidized (%)	T_{ox} (°C)
2×10^5	0.37	0.07 (0.07)	100	480	0.11 (0.30)	36	574
	0.97	0.19 (0.19)	100	540	0.40 (0.77)	52	656
2×10^4	0.37	0.07	100	485	0.11	36	575
	0.97	0.19	100	550	0.40	52	658
2×10^3	0.37	0.07	100	485	0.11	36	590
	0.97	0.20	105	570	0.40	52	670
90	0.37	0.065	95	487	0.11	36	605
	0.97	0.21	110	590	0.40	52	680
40	0.37	0.07	100	490	0.10	33	620
	0.97	0.25	131	610	0.30	39	700
7	0.37	0.08	114	490	0.08	27	630
	0.97	0.30	158	630	0.25	32	715

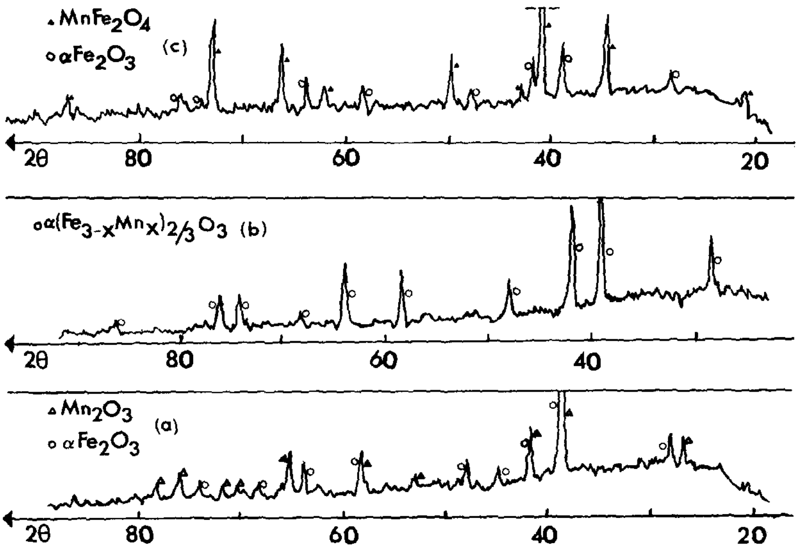

Fig. 5. X-ray diffraction patterns of phases formed at 600 °C as a function of oxygen pressure. a, $P_{O_2} > 10^3$ Pa; b, $10^3 > P_{O_2} > 2$ Pa; c, $P_{O_2} < 2$ Pa.

resulting from this transformation is highly dependent on the oxygen pressure and the composition factor x. On examination of powder diffraction patterns for the angular range from 10°–45° of the compounds heated at 600 °C (Fig. 5), a large number of lines was observed in comparison with the spinel phase.

For oxygen pressures above 10^3 Pa and for $x > 0.70$, the cation-deficient spinels were decomposed into the rhombohedral phase α-Fe_2O_3 and the orthorhombic phase Mn_2O_3 (Fig. 5, curve a). For the pressure range 10^3–2 Pa, the X-ray diagram exhibits the lines of α-Fe_2O_3 with only a slight shift (Fig. 5, curve b). Hence at this temperature, instead of decomposing into the respective oxides α-Fe_2O_3 and Mn_2O_3, the cation-deficient spinel is converted into the rhombohedral phase α-$(Fe_{3-x}Mn_x)_{2/3}O_3$ by reason of the solubility of Mn_2O_3 in α-Fe_2O_3. At lower oxygen pressures (below 2 Pa), the X-ray diffraction lines correspond to those of the spinel phase $MnFe_2O_4$ and α-Fe_2O_3. The formation of manganese ferrite at this temperature can be explained by the presence of Mn^{2+} ions that have not been oxidized. On the other hand, if the substitution extent x is low the rhombohedral phase α-$(Fe_{3-x}Mn_x)_{2/3}O_3$ is observed for the pressure range 2×10^5–1 Pa.

CONCLUSIONS

This study reveals that the oxidation of submicrometre-sized manganese-substituted magnetites occurs in several steps, depending highly on oxygen pressure. For the pressure range 2×10^5–90 Pa, and below 450 °C, a quantitative analysis of oxidizable cations such as Fe^{2+}, Mn^{3+} and Mn^{2+}, determined by DTG indicates that within the single-phase region of the spinel the octahedrally sited Fe^{2+} and Mn^{3+} ions are totally oxidized, whereas tetrahedrally sited Mn^{2+} ions exhibit only partial oxidation. From this analysis, the expression relating the defect concentration associated with manganese ions and the oxygen partial pressure has been given. Below 90 Pa the deviation from stoichiometry is also due to Fe^{2+} and Mn^{2+} ions which are partially oxidized or reduced. At higher temperatures (> 550 °C), it was established that the percentage of oxidized manganese ions depends also on oxygen pressure, and for low oxygen pressure (< 2 Pa) the formation of $MnFe_2O_4$ competes with the formation of α-Fe_2O_3. With increasing oxygen pressure, further oxidation of Mn^{2+} ions results in appearance of the rhombohedral α-$(Fe_{3-x}Mn_x)_{2/3}O_3$ phase for $2 < P_{O_2} < 10^3$ Pa and a mixture of the two phases α-Fe_2O_3 and Mn_2O_3 for $P_{O_2} > 10^3$ Pa.

REFERENCES

1 B. Gillot, M. El Guendouzi, P. Tailhades and A. Rousset, React. Solids, 1 (1986) 139.
2 P. Tailhades, M. El Guendouzi, A. Rousset and B. Gillot, C.R. Acad. Sci., Ser. 2, 299 (1984) 13.

3 P. Tailhades, A. Rousset, R. Bendaoud, A.R. Fert and B. Gillot, Mater. Chem. Phys. 17 (1987) 521.
4 M. Laarj, J. Pignone, M. El Guendouzi, P. Tailhades, A. Rousset and B. Gillot, Thermochim. Acta, 152 (1989) 187.
5 F.A. Kröger, The Chemistry of Imperfect Crystals, North-Holland, Amsterdam, 1964.
6 R. Morineau, Phys. Status Solidi A, 38 (1976) 659.